Applicability of the low-cost optical particle counter OPC-N3 for microphysical measurements of fog.

Katarzyna Nurowska[1], Moein Mohammadi[1], Szymon Malinowski[1], and Krzysztof Markowicz[1]

[1]Institute of Geophysics, Faculty of Physics, University of Warsaw, Warsaw, Poland

Correspondence: Katarzyna Nurowska (knurowska@fuw.edu.pl)

Abstract. Low-cost devices for particulate matter measurements are characterized by small dimensions and light weight. This advantage makes them ideal for drone measurements, where those parameters are crucial. However, they also have some issues, like the values of particulate matter from low-cost optical particle counters can be biased by high ambient humidity. In this article, we are evaluating low-cost optical particle counter Alphasense OPC-N3 for measuring the microphysical properties of

5   fog. This study aimed to show that OPC-N3 not only registers aerosols or humidified aerosols but also registers fog droplets.

The study was done on the rooftop of Institute of Geophysics, University of Warsaw, Poland, during autumn-winter 2021. To validate the results, the data from OPC-N3 were compared with data obtained from the reference instrument, which was Oxford Laser VisiSize D30. VisiSize D30 is a shadowgraph device able to register photos of individual droplets.

Taking into consideration the effective radius of droplets, it is possible to differentiate low-visibility situations between fog

10   conditions (which are not hazardous for people) from haze events, when highly polluted air can cause health risks to people.

The compared microphysical proprieties were liquid water content (LWC), number concentration (N_c), effective radius $< r_{eff} >$ and statistical moments of radius. The Pearson correlation coefficient for LWC was 0.91, N_c was 0.94, and for $< r_{eff} >$ was 0.63. Overall, these results suggest a good compliance between devices. However, the OPC-N3 has to be corrected in reference to professional equipment. To conclude, our study provides the foundation for a new application of the

15   optical particle counter Alphasense OPC-N3 within drones to measure the vertical profiles of the microphysical properties of fog.

1   Introduction

Fog is defined as a layer of water droplets (or ice crystals) near the Earth's surface, which reduces visibility to below 1 km. There are several different types of fog, depending on the cause which helps forming it, e.g., radiation fog, advection fog, and

20   valley fog. Radiation fog forms in the evening when the heat absorbed by the Earth's surface during the day is radiated into the air. The cold surface cools down the air causing condensation of water forming the first layer of fog. Fog phenomenon can affect small scale (valley fog) to size of the whole country.

It is a dangerous phenomenon for transport safety (Gultepe et al., 2015; Bartok et al., 2012), which causes not only increased road accidents, but also downtime of aircraft flights. This phenomenon affects the carriage of goods by land, air and maritime

25   transport, causing financial losses similar to those caused by extreme weather events (Kulkarni et al., 2019; Price et al., 2018).

The research by Vautard et al. (2009) shows that fogs in Europe have decreased significantly in the last 30 years. This can be the outcome of an increase in air temperature (Klemm and Lin (2016)). However, the fog decrease trend is spatially and temporally correlated with a negative trend in sulphur dioxide emissions, indicating that air quality policies have a significant impact on fog occurrence.

30   Particle matter (PM) is a suspension of particles of solids or liquids in the air such as dust, soot. Aerosol is an important component that contributes to fog formation. Decrease of PM can cause changes in fog occurrence or its microphysics. Fog is generated with relatively low super saturation (SS). Mazoyer et al. (2022) showed that the amount of activated aerosol depends more on the aerosol size than on its chemical composition. Numerical simulations conducted by Tsai et al. (2021) show that for urban aerosols (similar to the marine aerosol), a higher number density of aerosols resulted in more, but smaller droplets and

35   increased liquid water content (LWC). The effect of urban aerosols was more pronounced near the surface, where the aerosols were most concentrated. This result is consistent with Maalick et al. (2016), however, they also show that absorbing aerosols can lead to a decrease in LWC resulting in a shallower fog.

The decrease of fog events in Europe coincides with the reduction of particulate matter. Between 1998 and 2010, Barmpadimos et al. (2012) found that in Europe the concentration of PM_{10} (particulate matter of sizes less than 10 µm) decreased,

40   the mean trends were -0.4 $\mu g\,m^{-3}$ per year. According to Colette and Rouïl (2021) the median annual concentration of PM_{10} decreased by 40 % in Europe from 2000 to 2017. The decrease in $PM_{2.5}$ after 2008 was visible, but less pronounced. PM concentrations decrease due to the reduction of primary PM emissions, but also due to the reduction of PM precursors, such as SO_x, NO_x and NH_3. The mentioned studies agree with with Beloconi and Vounatsou (2021) where it was shown that during 14 years (2006-2019), the concentrations of PM_{10} and $PM_{2.5}$ decreased by 36.5% and 39.1%, respectively.

45   The decrease in PM_{10} and $PM_{2.5}$ is thanks to social awareness. Many countries introduced restrictions on the amount of PM_{10} and $PM_{2.5}$ emitted during the day and year. Due to the growing awareness of the community, the networks measuring the concentration of PM_{10} and $PM_{2.5}$ are growing (Considine et al., 2021; Feinberg et al., 2019). Consequently, there are increasingly inexpensive and simple PM sensors available on the market.

Low-cost optical particle counters (OPC) are based on measuring light scattering on suspended particles in the air. Light

50   scattering can be enhanced by water droplets. Thus, the reported values of PM are overestimated because of water uptake by the particles. It is shown that for some low-cost OPCs, the measured PM is dependent on ambient humidity (e.g., Liu et al., 2019; Wang et al., 2015; Badura et al., 2018; Jayaratne et al., 2018). To remove bias, the air should be dehumidified or correction methods should be applied, as proposed by Crilley et al. (2018).

Most of the fog studies focus on ground measurements or numerical modelling. Current weather forecasts have a problem

55   with high precision of fog forecasting. It is due to many processes in the lower boundary layer that are involved in its evolution. The processes that influence the development and duration of fog are, for example, droplet microphysics, aerosol hygroscopicity or radiation and turbulent processes (Gultepe et al., 2007). Fog is also affected by local surface conditions, as it develops in the immediate vicinity (Hu et al., 2017).

Microphysical models are based on microphysical parameters such as the total droplet number concentration (N_c), the mean

60   droplet diameter ($\overline{D}$) and LWC. Based on in situ measurements, many works provide the range for LWC $0.01 - 0.5\,\mathrm{g\,m^{-3}}$

(although the value typically does not exceed $0.2 \, \mathrm{g\,m^{-3}}$); N_c $10 - 500 \, \mathrm{cm^{-3}}$ and $\overline{D}$ $10 - 20 \, \mathrm{\mu m}$. However, these parameters show a large variability (e.g., Pruppacher and Klett, 2010; Liu et al., 2011; Tsai et al., 2021; Mazoyer et al., 2019, 2022).

The standard device used to measure fog microphysics is the Fog Monitor FM-120 from Droplet Measurement Technologies. It is an optical spectrometer that can measure the droplet size distribution (DSD(r)) from $2 \, \mathrm{\mu m}$ to $50 \, \mathrm{\mu m}$ in 23 channels (size bins). It can be used to obtain information on N_c, LWC, and visibility. This instrument is widely used to measure fog, allowing a consistent comparison of the results with those obtained in other studies (e.g., Weston et al., 2022; Gultepe et al., 2021; Mazoyer et al., 2019; Degefie et al., 2015; Gultepe et al., 2009).

Another in situ device is Cloud Droplet Probe 2 (CDP-2) that illuminates the droplets and measures the intensity of the forward-scattered light. This device was used, inter alia, during two campaigns oriented towards fog microphysics: High Energy Laser in Fog (HELFOG) project and the Toward Improving Coastal Fog Prediction (C-FOG) project (Wang et al., 2021). Droplets are measured in the range of $2 \, \mathrm{\mu m}$ to $50 \, \mathrm{\mu m}$ and N_c to $2000 \, \mathrm{cm^{-3}}$.

The alternative device used to retrieve the aerosol and fog particle size distribution is the Palas Welas-2000 particle counter. Palas Welas-2000 is a system capable of analysis of light scattering by a single particle. The device can measure particles in four ranges: $0.2 - 10 \, \mathrm{\mu m}$, $0.3 - 17 \, \mathrm{\mu m}$, $0.6 - 40 \, \mathrm{\mu m}$ or $2 - 100 \, \mathrm{\mu m}$. Palas Welas-2000 spectrometer was used in the ParisFog fog campaign Haeffelin et al. (2010). ParisFog lasted 6 months between October 2006 and March 2007. The measurements were taken at the SIRTA observatory 20 km south of Paris and a total of 154 hours of fog were recorded. The articles Elias et al. (2009a) and Elias et al. (2009b) focus on the amount of extinction caused by each particle mode in clear sky, haze (pre-fog) conditions and after fog onset. In clear sky, the extinction is caused in equal parts by the ultrafine and accumulation mode, during haze, the main role in the extinction plays the hydrated aerosol of the accumulation mode, and the fog droplet mode contributes $40 \, \%$ to the extinction.

Optical devices, such as the lidar or the celiometer, cannot penetrate thick fog to retrieve information about their vertical structure. On the contrary, radars based on micrometre wavelengths can penetrate the fog and measure the reflectivity and velocity structure (Hamazu et al., 2003). The HATPRO microwave radiometer (MWR) registers a vertical brightness temperature, where the highest resolution (200 m) is in the range of 0 to 2 km. Based on several brightness channels, the HATPRO artificial neural network algorithm inverts the radiance to estimate the vertical profiles of atmospheric temperature (T), relative humidity (RH), integrated water vapour, liquid water path (LWP) and liquid water content (LWC) vertical profile. SOFOG3D (SOuth west FOGs 3D experiment) was a project that was conducted from October 2019 to April 2020 in France over 300×300 km, where eight MWRs were used. The data from this campaign have been presented at scientific conferences so far (e.g., Martinet et al., 2021; Vishwakarma et al., 2021; Burnet et al., 2020). The reason for the use of MWR during the SOFOG3D campaign was the article Martinet et al. (2020), which showed the improvement of numerical weather prediction models by assimilation of MWR data.

The microphysical properties of fog are not the only ones that influence the life cycle of fog. Radiative heating and cooling are crucial to the development and decay of radiation fog. Wærsted et al. (2017) showed that for fog that has no cloud above and its liquid water path exceeds $30 \, \mathrm{g\,m^{-2}}$, the cooling of the fog by long-wave radiation can produce $40 - 70 \, \mathrm{g\,m^{-2}\,h^{-1}}$ liquid water by condensation. Furthermore, the heating of short-wave radiation can contribute significantly to the evaporation

Table 1. Days analysed.

Referred as	Measurement start [UTC]	Measurement stop [UTC]	Day / Night	Total minutes of fog
D-12.11	12.11.2021 19:11	13.11.2021 04:43	Night	150
D-16.11	16.11.2021 22:00	17.11.2021 07:21	Night	470
D-13.12	13.12.2021 09:03	13.12.2021 10:34	Day	50
D-14.12	14.12.2021 16:07	15.12.2021 08:20	Night	230
D-15.12	15.12.2021 17:58	16.12.2021 08:41	Night	130

by $10 - 15\,\mathrm{g\,m^{-2}\,h^{-1}}$ in thick fog in the middle of the day (winter). These results were obtained using MWR, cloud radar and celiometer.

Motivation for this work is a lack of devices that can perform in situ microphysical measurements of the vertical structure of the fog. For this purpose, miniature devices are needed that can be mounted on the Unnamed Aircraft Vehicle (UAV), balloons or cable cars. In this study, we propose a novel application of Alphasense OPC-N3 optical particulate matter. We postulate that OPC-N3 can be used to observe the microphysical properties of fog.

During this study, we observed fog near the city centre of Warsaw, at the Institute of Geophysics, University of Warsaw. Parameters such as LWC, N_c and the effective radius ($<r_{eff}>$) are examined. The results from Alphasense OPC-N3 were validated with the Oxford Laser VisiSize D30 (ShadowGraph instrument), which has already been successfully used to study cloud/fog microphysics (Nowak et al., 2021; Mohammadi et al., 2022).

The rest of this article is organized as follows: Sect. 2 describes data acquisition, the apparatus used and data processing. Section 3 shows the results of the comparison between OPC-N3 and ShadowGraph. Section 4 reports a case study of fog evolution during a night observation. Section 5 discusses the applicability of OPC-N3 to perform fog microphysics measurements.

2 Instrumentation and Methods

2.1 Apparatus

2.2 Data acquisition

The measurements were conducted in situ during the occurrence of fog on the roof (20 m above ground) of the Institute of Geophysics (52.21°N, 20.98°E, 115 m a.s.l.), Faculty of Physics, University of Warsaw, Poland. The OPC-N3 was mounted next to the Oxford Laser ViSize D30. In vicinity to those devices on the rooftop of Institute are mounted nephelometer Ecotech Aurora4000, CGR4 for incoming longwave (infrared) flux, CMP22 total incoming shortwave (solar) flux and Vaisala weather station WXT 520. Fog observations were carried out in the fall - winter period of 2021. A total of five days with fog were recorded, most of the fog occurred at night, and Table 1 summarises these events. During D-16.11, the longest period of fog occurred and was analysed in detail.

Table 2. ShadowGraph specification provided by Oxford Lasers Ltd. and by Nowak et al. Nowak et al. (2021). Alphasense OPC-N3 specification provided by Alphasense Ltd. and from Hagan et al. Hagan and Kroll (2020).

ShadowGraph		Lens magnification	$\times 4$
Camera sensor [pix × pix]	1952×1112	Magnification	6.12
Frame rate [fps]	30	Effective pixel size [µm]	0.90
Laser wavelength [nm]	808	Resolution [µm]	2.0
Laser pulse duration [µs]	0.1-5.0	Field of view [mm x mm]	1.75 x 1.00
Sampling	10 minutes	Depth of field [mm]	5.2
		Sample volume [cm^3]	0.0092
		Typical flow rate [cm^3 s^{-1}]	0.28
Alphasense OPC-N3			
Particle range	0.35-40	Laser wavelength [nm]	658
Bins	24	Viewing angle	$32° - 88°$
Sampling	1 minute	Refractive Index	$1.5 + 0i$
Weight [g]	105	Typical flow rate [cm^3 s^{-1}]	5.5

2.2.1 ShadowGraph

120 The VisiSize D30 is a ShadowGraph system manufactured by Oxford Lasers Ltd. ShadowGraph captures the photographs of particles passing through a volume between a laser head and a high-speed camera. This device is capable of distinguishing different sizes and shapes of particles in various suspensions in real time. The images are created by backlight illumination of a specific volume. The source of light is an infrared diode laser (808 nm). The maximum speed for capturing the droplets is defined by the camera, with the maximum frame rate being 30 fps. The manufacturer provides software for particle/droplet

125 image analysis. Detailed information on VisiSize D30 is described in two articles (Kashdan et al., 2003, 2004). The system allows retrieving microphysical properties such as shape, size, DSD(r), total droplet number concentration (N_c) and LWC.

ShadowGraph camera is equipped with different lens magnifications, and this adjustment can change the resolution of the sample volume. The manufacturer provides three calibrations: $\times 1$, $\times 2$, $\times 4$. For this study, the magnification of $\times 4$ was used, as it allows one to measure the smallest droplets. The effective pixel size for this magnification is 0.9 µm. The ShadowGraph

130 collects data in runs; one run was set to last 10 minutes. Table 2 presents further information on the ShadowGraph specification. VisiSize D30 ShadowGraph has already been successfully used to study cloud microphysics in the laboratory (Nowak et al., 2021) and in situ, in orographic clouds, i.e. in fog conditions over the mountains (Mohammadi et al., 2022).

2.2.2 OPC-N3

OPC-N3 is an optical particle counter developed by Alphasense Ltd. The device is constructed of a diode laser light (wavelength
135   658 nm) and an elliptical mirror that reflects the laser to a detector. The flow is perpendicular to the laser beam. By using a
fan to force the flow, the device can operate continuously without the need to periodically replace the pump filters. OPC-N3
measures the particle number concentration (PNC) in 24 bins, in a diameter range of 0.35 to 40 µm. The PNC measured by
the on-board algorithm is converted to PM_1, $PM_{2.5}$ and PM_{10}. OPC-N3 can measure the mass concentrations of particles up
to 2000 µg m^{-3}. The sensor returns information about the internal temperature and relative humidity. More information on the
140   Alphasense OPC-N3 specification is provided in Table 2, more details about OPC-N3 can be found in Hagan and Kroll (2020).

2.3 Data processing

2.3.1 Fog detection

To automatically retrieve data concerning fog events, calculations were performed to obtain the minimum concentration of
droplets needed to create a fog. Koschmieder formula (Equation 1) relates visibility (VIS) to the scattering coefficient σ.

$$\mathrm{VIS} = \frac{\ln 50}{\sigma} \qquad (1)$$

The scattering coefficient σ is defined by the equation:

$$\sigma = \pi \int r^2 Q_e \mathrm{DSD}(r) dr \qquad (2)$$

where r - droplet radius, DSD(r) - droplet size distribution and Q_e is the efficiency coefficient for extinction. To estimate the
minimum N_c, it was assumed that fog consists of a monodisperse distribution of droplets with radius 9.76 µm (effective radius
150   of droplets measured by ShadowGraph). From the Mie theory for the radius 9.76 µm the Q_e was calculated to be 2.17.

Based on Equations 1) and 2) the minimum concentration of droplets necessary to cause fog was obtained - 6.03 cm^{-3}. For
calculations of the microphysical properties of fog data from ShadowGraph for which the droplet concentration is greater than
or equal to 6.03 cm^{-3} were taken into account. During five days, 103 runs (each of 10 min) with detected fog were obtained.

2.3.2 ShadowGraph depth-of-field

155   To calculate the droplet number concentration, ShadowGraph needs information on the depth of field (DOF). Kashdan et al.
(2003) proposed a linear dependence of the DOF for the particle diameter in the range $18 - 145$ µm. However, Nowak et al.
(2021) showed that for smaller droplets, focus rejection criteria play a role and must be taken into account in the DOF formula.
In this study, to obtain results depending on the DOF, the formula of Nowak et al. (2021) was used. $z_{95|Di}$ is DOF proposed by
Nowak et al. (2021) which depends on the diameter of the droplet, a_i are the parameters, respectively, of the lens magnification
160   given by the manufacturer.

$$z_{95|D_i} = \frac{0.95}{(1 - 0.95 a_3)(a_1 D_i + a_2)} \frac{\pi}{4} \frac{(D_i + a_4 + a_5)^2}{pix^2} \qquad (3)$$

The total volume measured for each droplet is the following:

$$V_i^{ind} = 2z_{95|D_i}(L_x - D_i)(L_y - D_i) \tag{4}$$

where i denotes the iterations of the measured droplets, D_i its diameter in µm, L_x and L_y denote the size of the effective area
of the camera sensor in µm.

2.4 Uncertainty of the measurement

The data from ShadowGraph were integrated every 10 minutes. To calculate the uncertainty of the values (LWC, N_c, mean
radius) calculated from ShadowGraph, it was assumed that the uncertainty is only influenced by the effective pixel size of
ShadowGraph of 0.9 µm. The formula for the DOF depends on the diameter of the droplet. The uncertainty of a given variable
was calculated using the formula for the propagation of uncertainty.

Data from OPC-N3 were collected every 10 seconds, averaged to 1 minute and then averaged every 10 minutes to compare
them with ShadowGraph. As uncertainty of the OPC-N3 data, the standard deviation was used, obtained by averaging the data
over 10-minute periods.

2.4.1 Scope of compliance between OPC-N3 and ShadowGraph

Figure 1 (**a**) shows the volume droplet size distribution (vDSD(r)) and (**b**) droplet size distribution (DSD(r)) of OPC-N3
and ShadowGraph. The data was averaged over one hour. Aphasense OPC-N3 manual specifies that OPC-N3 record droplet
radiuses in the range of 0.175 to 20.000 µm. On the Fig. 1 can be seen that the last bin of OPC-N3 registers a much grater mass
of droplets than it would appear from the distribution. This indicates that the last bin has not properly assigned its right edge.
In the last bin of OPC-N3 the particles of radiuses larger than 20.00 µm are also counted.

The last OPC-N3 bin contains a significant part of LWC, for this reason it was not excluded from the analysis. However,
a new mean radius ($< r >$) for this bin was estimated based on ShadowGraph data. From all ShadowGraph data of fog was
created one histogram of DSD, the mean volume radius ($< r_V >$) was calculated for droplets bigger than 18.5 µm. The obtained
$< r_V >$ is 21.76 µm. Based on this calculation the lower boundary of OPC-N3 last bin is set as 18.5 µm, the mean radius is set
to 21.76 µm and the upper boundary is set as 25.02 µm (the upper limit is set in such a way that the center of the bin falls on
the mean radius). The Fig. 1 (**c**) shows how the vDSD looks after adjustment of the last bin of OPC-N3.
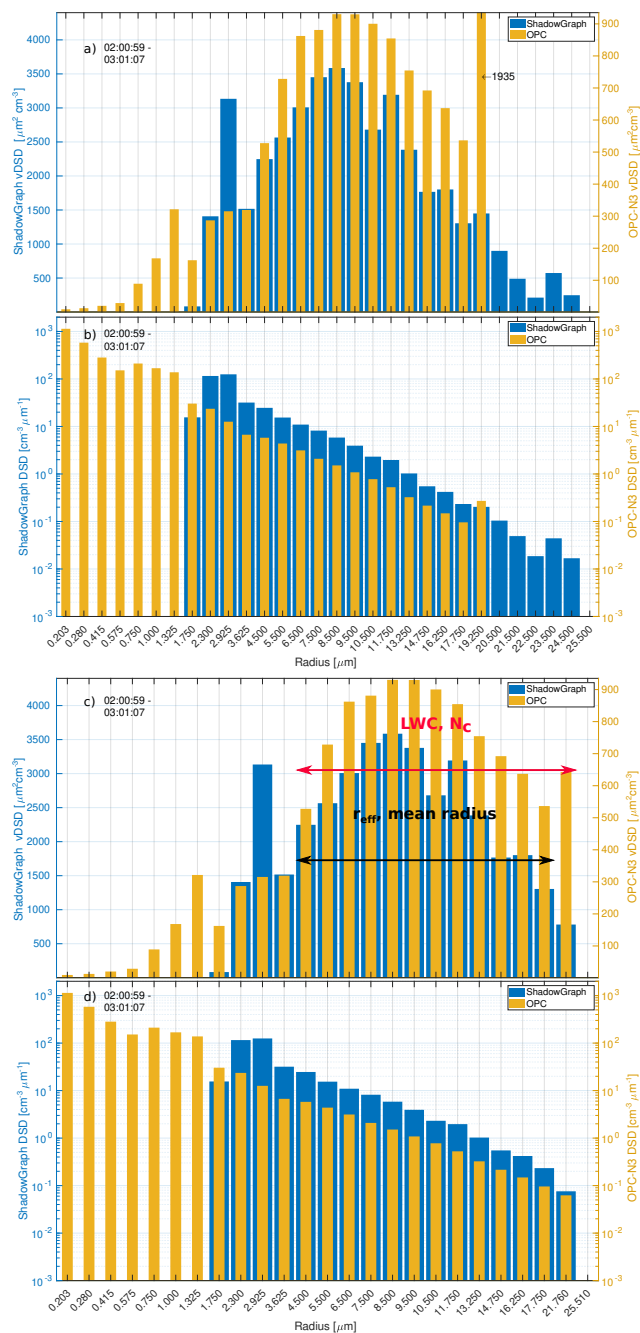
Figure 1. The droplet size distribution DSD(r) - Fig. (**b**) and (**d**)) and volume droplet size distribution vDSD(r) - Fig. (**a**) and (**c**) of OPC-N3 and ShadowGraph. In yellow are shown the values obtained for each bin of OPC-N3, in blue are shown ShadowGraph data, aggregated into the same bins as OPC-N3. The data were averaged by one hour (17 November 2021, 02:00:59 - 03:01:07). The right axis corresponds to OPC-N3. Fig. (**a**) and (**b**) represent the bins from OPC-N3 as they are provided by manufacturer. In Fig. (**c**) and (**d**), the last bin of OPC-N3 has bin adjusted and its range is $(18.5 - 25.02]$ μm. In Fig. (**c**), in red the range of OPC-N3 bins taken into account for the calculations of LWC and N_c is shown, and in black for $< r_{eff} >$ and mean radius. The number 1935 on Fig. (**a**) indicates the value of last bin of OPC-N3.

Table 3. The range of droplet radiuses which was taken into account for the calculation of microphysical proprieties of fog.

	LWC, N_c	$< r_{eff} >, < r >, < r_s >, < r_V >$
droplet radii [µm]	4.00 - 25.02	4.00 - 18.50

Oxford Lasers state that the minimum value of the diameter that can be imaged by the ShadowGraph for a magnification of $\times 4$ is 2 µm. The minimum diameter of fog droplet registered by ShadowGraph was 3.47 µm.

ShadowGraph spectrum has a peak in the bin of droplet mean radius 2.925µm. This pick is not visible in the OPC-N3 data. It appears to be a problem in recognising the actual size of small droplets by algorithm. The pixel size of ShadowGraph is 0.9 µm, leading to misinterpretation of droplets of size of 2-3 pixels. In the article of Kashdan et al. (2003) there is a peak in the droplet distribution function for the bin with the smallest droplets. This is explained by the misclassification of small unfocused droplets. Identification of the droplets and their size is done by distinguishing the brightness between the shadow of the drop and the brightness of the background pixels. For fuzzy droplets, the difference is small, making it difficult to classify the droplets to the correct size. In our analysis the droplets below radius of 4 µm where excluded.

During the five days of the study, fog was observed for 17.2 hours. Microphysical parameters such as N_c, LWC, $< r_{eff} >$ and mean radius were calculated. For those calculations, droplets from range 4 µm to 25.024 µm where taken into account for both devices. In the case of OPC-N3, it corresponds to bins from 12 to 24. The bin 24 was taken into account as it contains a significant amount of LWC, but after adjusting its mean radius to 21.76 µm. Droplets smaller than 4 µm where excluded from the comparison as ShadowGraph has problems in classifying them correctly.

For the comparison of $< r_{eff} >$ and mean radius, only the droplets from range 4 µm to 18.5 µm were taken into account for ShadowGraph and OPC-N3 (bins 12 to 23 of OPC-N3), as in this range the registered sizes of droplets from both devices overlap without any adjustments. The droplet radius range, taken into account for each microphysic parameter, is shown in Table 3.

Particles in OPC-N3 are assigned to the size bins based on the amount of light scattered. In Mie theory, the amount of light scattered can be linked to a specific size of a particle; to be able to use Mie theory, one needs to assume an appropriate refractive index (RI) of a particle. In OPC-N3, the manufacturer set the RI_{OPC} at $1.500 + 0.00i$. The refractive index of pure water - $\text{RI}_{water} = 1.331 + 0.000i$ (Hale and Querry, 1973) - is different from the one assumed in OPC-N3, which can lead to incorrect assignment of the droplets to the correct bin based on its radius. We analysed the effect of recalculating the assignment of droplets to specific bins using RI_{water}. As a result, we have obtained that the vDSD spectrum of OPC-N3 and ShadowGraph after RI correction does not overlap as well as when it was assumed RI_{OPC}, however due to the greater representation of bigger droplets a better comparison of LWC between the devices was obtained.

2.4.2 OPC-N3 temperature and relative humidity

Alphasense OPC-N3 reports temperature (T) and relative humidity (RH). The sensors are mounted inside the device. The registered values were compared with Vaisala WXT520, which is mounted on the roof of the Institute of Geophysics and

215 measures ambient T and RH. As seen on Fig. 2 (**a**) the T inside OPC-N3 is approximately $6°C$ higher than that of Vaisala
WXT520. Probably the circuit board system is heating the inside of the device. This causes a drop in humidity within OPC-N3.
When comparing the RH of OPC-N3 with Vaisala WXT520, it is seen that the RH within OPC-N3 is lower around 20 %.
The measurements presented were taken during the night and early morning. During the night, the value from OPC-N3 seems
to be shifted by a constant value in comparison with Vaisala WXT520. The temperature and RH registered by OPC-N3 start
220 rapidly changing after sunrise (6:00 UTC). The OPC-N3 is made of black plastic which probably is heated by sunlight, the
higher temperature of the body affects the inside humidity. This leads to the conclusion that the T and RH reported by OPC-N3
cannot be used as the values of ambient conditions and can not be easily corrected. Furthermore, a higher T and lower RH
within OPC-N3 may have an impact on the droplet size due to the evaporation process.
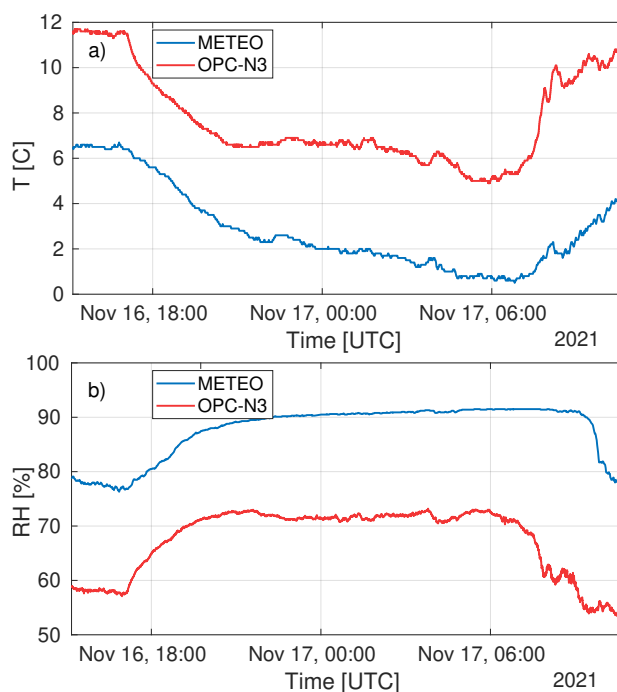
Figure 2. Comparison between OPC-N3 (red line) with Vaisala WXT520 (blue line) of (**a**) temperature (T) and (**b**) relative humidity (RH).
Devices mounted on the roof of the Institute of Geophysics, sunrise at 6:00 UTC.

3 Results

3.1 Microphysical properties of fog

3.1.1 Liquid water content

LWC results are shown on Fig. 3 (**a**). The LWC calculated from ShadowGraph ranges from 0 to $0.2\,\mathrm{g\,m^{-3}}$. The comparison between OPC-N3 and ShadowGraph shows a linear relationship between devices. The OPC-N3 values are almost two times lower than those from ShadowGraph. The Pearson correlation coefficient (PCC) is 0.91.

Values such as LWC, N_c, droplet diameter statistics obtained from OPC-N3 can be corrected using a linear regression curve of the form $y = ax + b$, where x is the measured value from OPC-N3, a and b are calculated coefficients and y is the measured value from ShadowGraph. The linear regression coefficients, PCC and RMSE for LWC are presented in Appendix A Table A1.
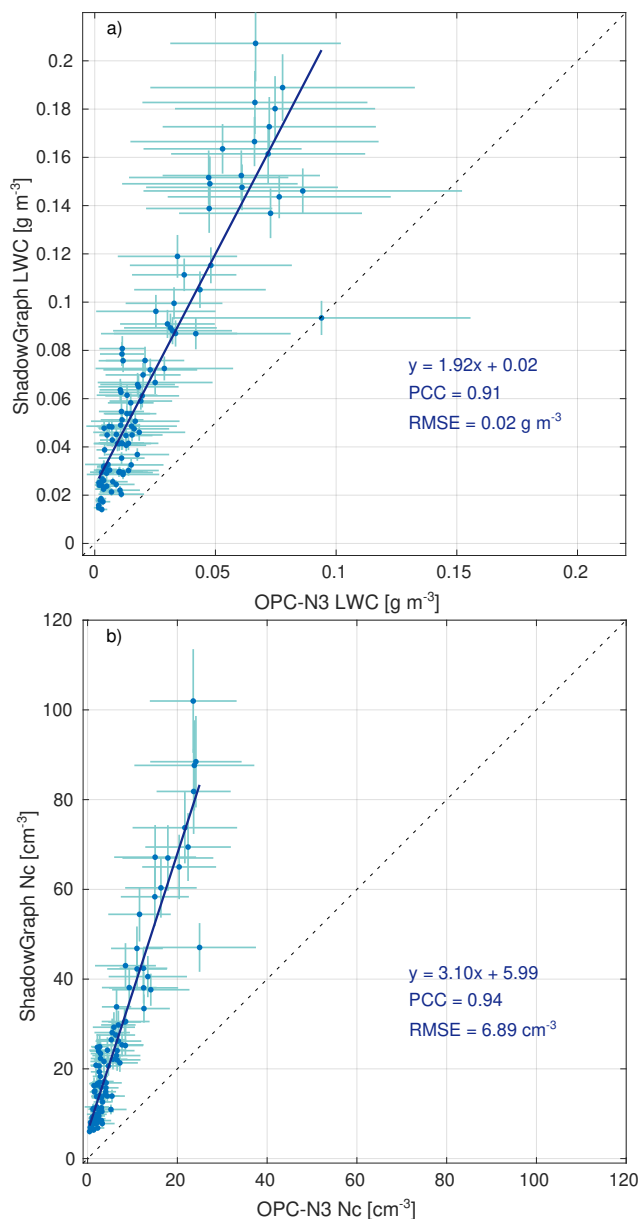
Figure 3. Comparison between ShadowGraph and OPC-N3 of (**a**) liquid water content (LWC) (**b**) total droplet number concentration (N_c). Each point represent value measured over 10 minutes period. Blue points represent data retrieved from the devices, solid deep blue line represent linear fit to the data, bars represent the estimation of standard deviation.

3.1.2 Total number concentration

The droplet number concentration is shown in Fig. 3 (**b**), the values span almost from 10 to around 100 cm^{-3} for ShadowGraph.
235 There is a high Pearson correlation coefficient equal to 0.94 for the comparison with OPC-N3. The values obtained from OPC-

© BY

N3 are lower than those obtained from ShadowGraph. The linear regression coefficients, PCC and RMSE for N_c are presented in Appendix A Table A1.

3.1.3 Droplet diameter

Four different droplet diameter statistical moments were calculated. The arithmetic mean $< r >$, the surface mean $< r_S >$, the volume mean $< r_V >$ and the $< r_{eff} >$. The values were calculated using a formula for statistical moments. To calculate $< r_{eff} >$, the following formula was used:

$$< r_{eff} >= \left(\sum_{i=1}^{m} r_i^3 \cdot N_i \right) \cdot \left(\sum_{i=1}^{m} r_i^2 \cdot N_i \right)^{-1}, \tag{5}$$

where N_i in the case of OPC-N3 is the concentration of droplets in the volume of the bin, m denotes the number of bins. For ShadowGraph, m denotes the number of droplets and $N_i = V_i^{-1}$ where V_i is the volume in which the droplet was measured.

Figure 4 shows the $< r_{eff} >$ and Fig. 5 (**a**) the mean radius, (**b**) the mean surface radius and (**c**) the mean volume radius. The $< r_{eff} >$ is between 8.05 and 11.71 µm for ShadowGraph. There is a modest correlation coefficient between the devices for all mean radiuses. The linear regression coefficients, PCC and RMSE for $<< r_{eff} >>$ are presented in Appendix A Table A1.
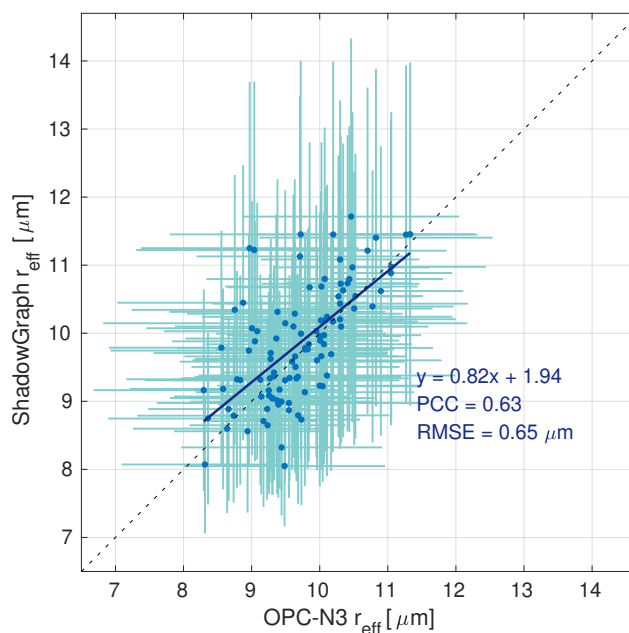
Figure 4. Comparison between ShadowGraph and OPC-N3 of $< r_{eff} >$ [µm]. Each point represent value averaged over 10 minutes, the bars represent the estimation of standard deviation. Blue points and lines represent data retrieved from the devices, solid deep blue line represent linear fit to the data.
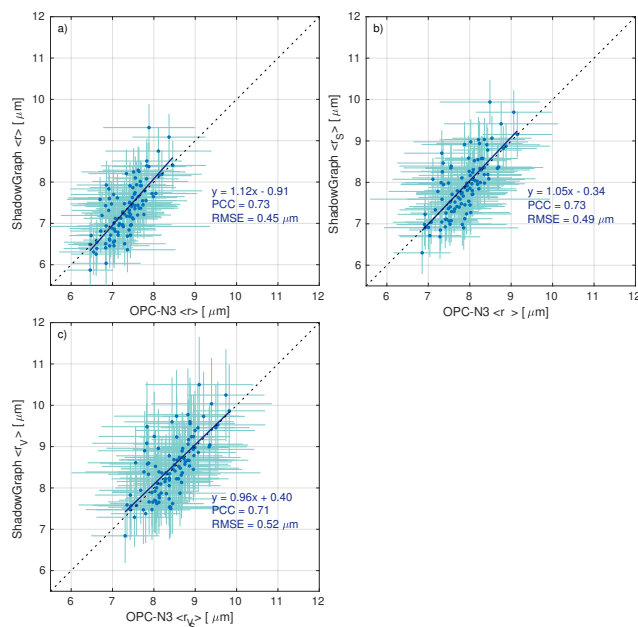
Figure 5. Comparison between ShadowGraph and OPC-N3 for (**a**) mean radius [µm], (**b**) mean surface radius [µm], (**c**) mean volume radius [µm]. Each point represent value averaged over 10 minutes, the bars represent the estimation of standard deviation. Blue points and lines represent data retrieved from the devices, solid deep blue line represent linear fit to the data, bars represent the estimation of standard deviation.

4 Case study

4.1 Overview of weather conditions

250 In this section, the evolution of fog which occurred at night November 16, 2021 is studied. On 16 November 2021, Poland was in the saddle region, between two highs over the North Atlantic and Ukraine. The anticyclone above Ukraine moved towards the Caspian Sea, causing the pressure to drop from 1008 hPa at 18:00 UTC to 1004 hPa around 07:00 UTC on November 17, 2021. Atmospheric conditions at the saddle point resulted in a decrease in wind speed during the measurements. The wind blowing from the direction $150°$ was on average $2.2\,\mathrm{m\,s^{-1}}$, which favoured the formation of fog.

255 Fog started to form around 21:15 UTC. The sky was clear before fog occurrence (infrared incoming surface flux was around $250\,\mathrm{W\,m^2}$ before 20 UTC). Infrared flux started to rise around 21 UTC, and it dropped around 22:16, suggesting a temporary disappearance of fog. Approximately at 4:00 UTC, the infrared flux started to decrease, and after sunrise the total flux was increasing - the line representing the total flux is jagged, which suggests that in the morning above the fog was a layer of thin clouds.

260 From 18:00 UTC, on 16 November 2021, the air temperature decreased from $5.4°C$ to a minimum of $0.5°C$ just before 07:00 UTC the next day. The temperature then started to increase and the process of dissipating the fog started. In Appendix B

Fig. B1 shows in detail the atmospheric situation on the measurement site and Appendix B Fig. B2 presents the radiosounding from 00 UTC 17 November 2021 from Legionowo, which is near Warsaw city.

In Appendix B Fig. B1 (**a**) shows the scattering coefficient at 525 nm measured by Aurora 4000 nephelometer at dry conditions (the humidity inside Aurora 4000 during the measurements was below 30 %). The values increased from 178 Mm^{-1} at 18:00 UTC to 250 at 19:30 UTC, then oscillated between 250-260 Mm^{-1} until 23:15 UTC, then continuously decreased to 170 Mm^{-1} at 07:00 UTC. Values above 200 Mm^{-1} suggest moderate smog conditions. The increase in the scattering coefficient after 18:00 UTC was probably due to air pollution caused by the activation of the house heating system and traffic emissions.

The PM values obtained from OPC-N3 are presented in Fig. 6. The PM_1 was around 17 $\mathrm{\mu g\,m^{-3}}$ at 18:00 UTC and increased to 125 $\mathrm{\mu g\,m^{-3}}$ at 23:00 UTC, then the PM_1 value decreased. PM_{10} data exhibit a different behaviour from PM1. Between 21:00 and 22:30 UTC, 22:45 and 04:00 UTC, 04:20 and 06:10 UTC, episodes of significant increase and decay in PM_{10} value have been observed. For each episode, PM_{10} reached, respectively (14960, 12550, 6897 $\mathrm{\mu g\,m^{-3}}$). A similar pattern is observed in $PM_{2.5}$ but less pronounced (1354, 1148, 893 $\mathrm{\mu g\,m^{-3}}$). Such values are unrealistic for Warsaw City, the values are biased due to high humidity and fog droplet contamination. These episodes correspond to three periods of fog events. In Fig. 6 (**b**) the estimated values of LWC are presented for OPC-N3 and ShadowGraph.

The data collected from OPC-N3 allows to calculate the effective radius. In Appendix B Fig. B1 (**b**) it is shown the effective radius calculated from all the droplets that have radius bigger than 1.15 μm ($r_{eff}^{1.15}$). The $r_{eff}^{1.15}$ rapidly increases after the fog onset. This parameter can be used as an automatic detection of fog events. When there are high concentrations of PM, based on $r_{eff}^{1.15}$, it is possible to distinguish an episode of haze from an episode of fog.
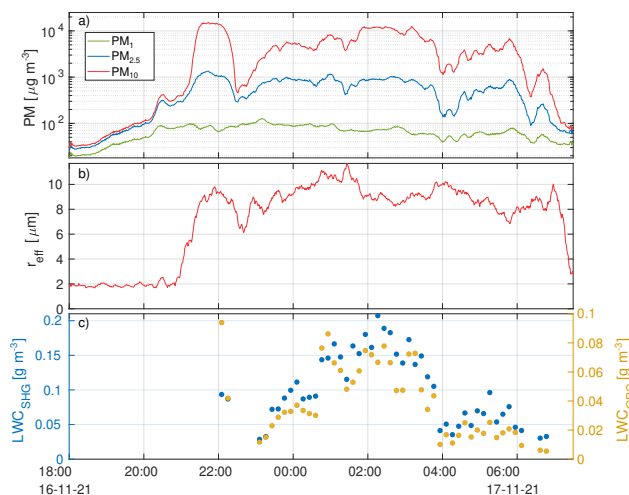
Figure 6. Situation over the night of November 16, 2021: (**a**) PM_1, $PM_{2.5}$ and PM_{10} obtained from Alphasesnse OPC-N3. The data from this instrument is collected every minute, and later a running mean over ten minute window was applied to smooth the data. (**b**) Effective radius calculated from OPC-N3 for droplets (radiuses from 1.15 µm where taken into account). (**c**) LWC obtained from ShadowGraph and OPC-N3. The values were calculated every ten minutes. LWC was calculated only for fog occurrence set as droplet concentration is higher than or equal 9.73 cm^{-3}.

4.2 Evolution of the droplet spectrum

In this subsection, the evolution of the droplet spectrum is shown for the period between 22:00 UTC November 16 and 07:00 UTC November 17. Figure 7 shows the vDSD(r) for OPC-N3 and ShadowGraph. In one plot, the data for the average of one hour are shown.

285   Figure 7 shows a relatively good agreement between devices on the behaviour of the droplet spectrum. During the night of 16 November, the first fog event occurred from 21:00 to 22:20 UTC. Due to some connection errors, the ShadowGraph was set at 22:00 UTC. Moreover, during the first 10 minute run, probably due to the steamed lens, it did not recognise all the droplets that passed through it.

The spectrum obtained from OPC-N3 consists of a two-mode distribution. The first mode has a maximum for bin mean
290   radius 1.33 µm and its location remains steady at night. The second mode pick during hours 23:00 - 02:00 UTC moves from 11.75 µm to 14.75 µm. During this time, the fog evolves and the value of the vDSD(r) increases. The maximum intensity of the fog is observed at 02:00 - 03:00 UTC and the pick of the second mode rapidly changes to 8.50 µm. After 3:00 UTC, the second mode of droplet distribution flattens out and the fog starts to disappear. The data obtained from ShadowGraph follow the same pattern and the values obtained from ShadowGraph are greater. During 02:00 - 03:00 UTC, the maximum value of
295   the vDSD(r) was 930 $\mathrm{µm}^2\,\mathrm{cm}^{-3}$ for OPC-N3 and 3586 $\mathrm{µm}^2\,\mathrm{cm}^{-3}$ for ShadowGraph.
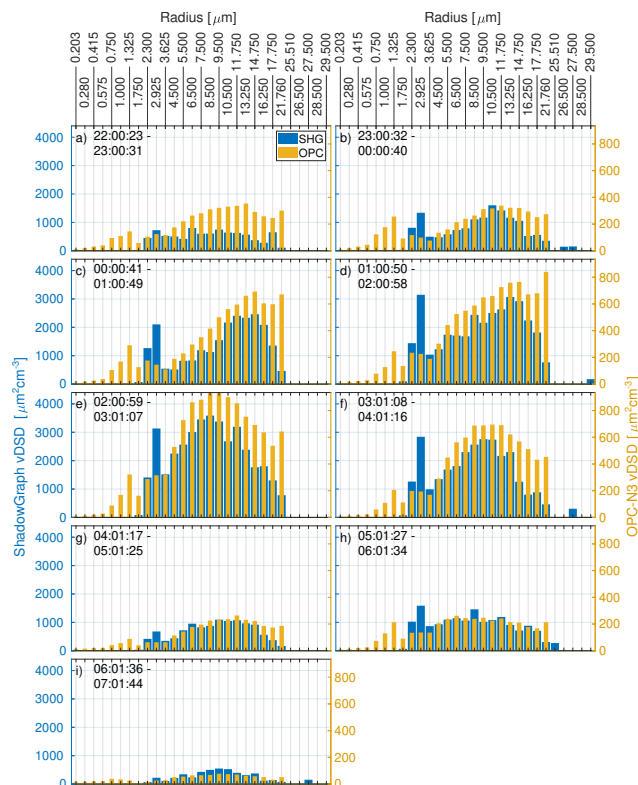
Figure 7. Volume droplet size distribution (vDSD(r)). In blue are shown data obtained ShadowGraph, in yellow from OPC-N3. Figures from (**a**) till (**i**) represent consecutive hours between 22:00 UTC November, 16 and 07:00 UTC November, 17.

5 Conclusions

The low-cost optical particle counter Alphasense OPC-N3 was tested for its application in the measurement of fog droplets and compared to Oxford Lasers VisiSize D30 ShadowGraph. There were some limitations in comparing the radius ranges of both devices. The manual provided by Oxford Lasers reports that the minimum radius resolution of ShadowGraph is 1.01 µm. However, during the measurements, ShadowGraph did not record droplets smaller than 1.73 µm. Interestingly, the results reveal that there were non-physical concentrations of droplets in bin (2.6 -3.24 µm). As we stated in Sec. 2.4.1 this peak probably comes from noise and problems with the wrong diameter assignment of small defocused droplets. We conclude that the minimal practical radius that can be measured by ShadowGraph is approximately 3.5-4 µm for lens magnification ×4.

The range of comparison between the devices ranged from a radius of approximately 4 µm to 18.5 / 25.02 µm. To better illustrate the data, we present the results as a vDSD(r). An interesting aspect that has emerged from this analysis is that the last bin (diameter $18.5 - 20$ µm) of OPC-N3 counts not only drops to 20 µm, but also larger. We estimated based on ShadowGraph data that the last bin of OPC-N3 for this analysis collects droplets from $18.5 - 25.02$ µm. Because this instrument is used mainly for aerosol measurements, which are usually not present at this size, this problem has not been described before.

Badura et al. (2018) showed that the previous version of Alphasense OPC overestimates PM values in high humidity. Our
310 results are in line with this article, OPC-N3 in the case of high humidity $RH = 80 - 90\,\%$ can overestimate PM values. During
this study, the value of PM_{10} reached $15185\,\mathrm{\mu g\,m^{-3}}$. Such high values cannot be explained only by the higroscopic growth of
aerosols. The high PM values are associated with fog occurrence and are a result of the count of fog droplets by OPC-N3. The
main point of this article was to verify the hypothesis that the values are overestimated because OPC-N3 counts fog droplets.

The LWC, N_c, $< r_{eff} >$ and the statistical moments of radius were calculated based on the data obtained from OPC-N3. The
315 values were compared with those retrieved from ShadowGraph. Overall, these results suggest that there is a high correlation
between OPC-N3 and ShadowGraph. OPC-N3 can be used to measure fog microphysics; however, the values reported by
OPC-N3 need to be corrected.

The OPC-N3 lowers the values compared to ShadowGraph; in the case of LWC the values are 1.92 times lower and in the
case of N_c 3.10 times lower. As OPC-N3 uses a default RI index for radius calculations, it was investigated whether applying
320 the correction of the RI index would improve the compatibility of the instruments. After correction, an improvement in LWC
was observed; OPC-N3 data were 1.15 times smaller than the ShadowGraph values. As shown in Sect. 2.4.2 within OPC-N3
T is higher by $6°C$ and RH is lower by $20\,\%$ compared to ambient T and RH. Inside OPC-N3, there are favourable conditions
for droplet evaporation, which may be the reason for the observed lower LWC and N_c.

OPC-N3, due to its dimensions and low weight, can be mounted on UAVs, cable cars or balloons. Such works have been
325 performed with small OPCs by Posyniak et al. (2021); Habeck et al. (2022); Girdwood et al. (2020). The main objective of
that research was to investigate changes in PM in the vertical profile. Our work presents a new applicability of OPC-N3 within
drones to measure the vertical profiles of the microphysical properties of fog. Additionally, using the AE-51 device on flying
platforms, it would allow to estimate the impact of smog on the development of fog. Another application of our study could
be to produce cheap fog detection systems in airports or automatic fog monitoring systems on roads. Taking into consideration
330 the effective radius of droplets received from OPC-N3, it is possible to differentiate the low-visibility situations between fog
conditions (which are not hazardous for people) from haze events, when highly polluted air can cause health risks to people.

Code and data availability. The results presented in this study were obtained with the use of the Oxford Lasers VisiSize D30 software
version 6.5.39 and code developed by the authors in the MATLAB environment. The latter are available from the authors upon request. The
data presented in this study are available from the authors on request.

Appendix A

335

Table A1. The linear regression coefficients, Pearson's correlation coefficient (PCC) and the root mean square error (RMSE) for LWC, N_c, $< r_{eff} >, < r >, < r_s >, < r_V >$. The linear regression was obtained for data without RI correction and with RI correction applied.

		No RI correction			RI correction	
LWC	a	1.923 ± 0.085		a	1.148 ± 0.050	
	b	0.024 ± 0.003	$[\text{gm}^{-3}]$	b	0.024 ± 0.003	$[\text{gm}^{-3}]$
	PCC	0.914		PCC	0.915	
	RMSE	0.020	$[\text{gm}^{-3}]$	RMSE	0.020	$[\text{gm}^{-3}]$
N_c	a	3.098 ± 0.108		a	2.702 ± 0.090	
	b	5.989 ± 0.942	$[\text{cm}^{-3}]$	b	6.350 ± 0.967	$[\text{cm}^{-3}]$
	PCC	0.944		PCC	0.948	
	RMSE	6.890	$[\text{cm}^{-3}]$	RMSE	7.073	$[\text{cm}^{-3}]$
$< r_{eff} >$	a	0.816 ± 0.099		a	0.668 ± 0.088	
	b	1.939 ± 0.959	$[\mu\text{m}]$	b	2.694 ± 0.981	$[\mu\text{m}]$
	PCC	0.635		PCC	0.605	
	RMSE	0.655	$[\mu\text{m}]$	RMSE	0.751	$[\mu\text{m}]$
$< r >$	a	1.124 ± 0.104		a	0.894 ± 0.083	
	b	-0.915 ± 0.766	$[\mu\text{m}]$	b	0.125 ± 0.663	$[\mu\text{m}]$
	PCC	0.731		PCC	0.730	
	RMSE	0.452	$[\mu\text{m}]$	RMSE	0.472	$[\mu\text{m}]$
$< r_s >$	a	1.047 ± 0.098		a	0.837 ± 0.080	
	b	-0.335 ± 0.773	$[\mu\text{m}]$	b	0.613 ± 0.695	$[\mu\text{m}]$
	PCC	0.728		PCC	0.721	
	RMSE	0.487	$[\mu\text{m}]$	RMSE	0.520	$[\mu\text{m}]$
$< r_V >$	a	0.961 ± 0.096		a	0.772 ± 0.080	
	b	0.403 ± 0.808	$[\mu\text{m}]$	b	1.291 ± 0.758	$[\mu\text{m}]$
	PCC	0.707		PCC	0.692	
	RMSE	0.522	$[\mu\text{m}]$	RMSE	0.568	$[\mu\text{m}]$

Appendix B
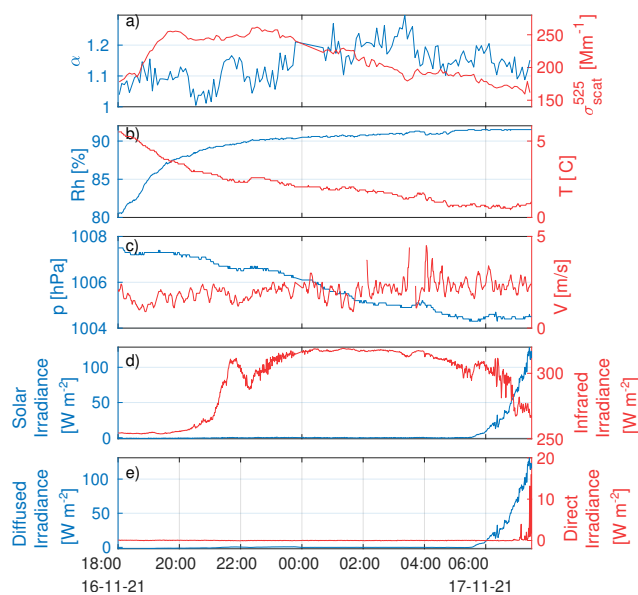
Figure B1. Situation over the night of November 16, 2021: (**a**) Scattering coefficient (σ_{scat}^{525} and Ångström exponent obtained from Ecoteh Aurora 4000. The data from this instrument is collected every five minutes. (**b**) Temperature (T) and relative humidity (RH) obtained from Vaisala WXT520. The data from this instrument is collected every minute. (**c**) Local pressure (p) and mean wind velocity (V) obtained from Vaisala WXT520. (**d**) Total and infrared irradiance, (**e**) diffused and direct irradiance.
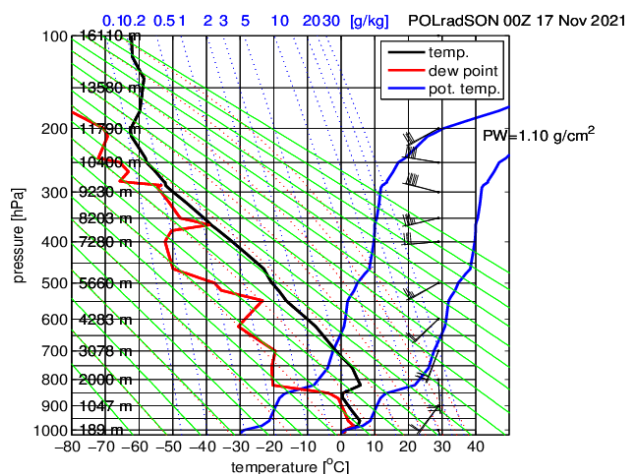
Figure B2. Radio sounding from 00 UTC 17 Nov., 2021 from Legionowo (near Warsaw), Poland.

Author contributions. SM and KM planned the campaign; KN, MM, KM performed the measurements; KN analyzed the data; KN wrote the manuscript draft; KN, MM, SM, KM reviewed and edited the manuscript.

Competing interests. Some authors are members of the editorial board of journal Atmospheric Measurement Techniques. The peer-review
340   process was guided by an independent editor, and the authors have also no other competing interests to declare.

Acknowledgements. This research was funded by the National Science Centre (NCN), Poland, grant number UMO-2017/27/B/ST10/00549.

References

Badura, M., Batog, P., Drzeniecka-Osiadacz, A., and Modzel, P.: Evaluation of Low-Cost Sensors for Ambient PM2.5 Monitoring, Journal of Sensors, 2018, https://doi.org/10.1155/2018/5096540, 2018.

Barmpadimos, I., Keller, J., Oderbolz, D., Hueglin, C., and Prévôt, A. S. H.: One decade of parallel fine ($PM_{2.5}$) and coarse (PM_{10}–$PM_{2.5}$) particulate matter measurements in Europe: trends and variability, Atmospheric Chemistry and Physics, 12, 3189–3203, https://doi.org/10.5194/acp-12-3189-2012, 2012.

Bartok, J., Bott, A., and Gera, M.: Fog Prediction for Road Traffic Safety in a Coastal Desert Region, Boundary-Layer Meteorology, 145, https://doi.org/10.1007/s10546-012-9750-5, 2012.

Beloconi, A. and Vounatsou, P.: Substantial Reduction in Particulate Matter Air Pollution across Europe during 2006–2019: A Spatiotemporal Modeling Analysis, Environmental Science & Technology, 55, 15 505–15 518, https://doi.org/10.1021/acs.est.1c03748, pMID: 34694135, 2021.

Burnet, F., Lac, C., Martinet, P., Fourrié, N., Haeffelin, M., Delanoë, J., Price, J., Barrau, S., Canut, G., Cayez, G., Dabas, A., Denjean, C., Dupont, J.-C., Honnert, R., Mahfouf, J.-F., Montmerle, T., Roberts, G., Seity, Y., and Vié, B.: The SOuth west FOGs 3D experiment for processes study (SOFOG3D) project, in: EGU General Assembly 2020, Online, 4–8 May 2020, EGU2020-17836, https://doi.org/https://doi.org/10.5194/egusphere-egu2020-17836, 2020.

Colette, A. and Rouïl, L.: ETC/ATNI Report 16/2019: Air Quality Trends in Europe: 2000–2017. Assessment for surface SO2, NO2, Ozone, PM10 and PM2.5—Eionet Portal., Eionet Report - ETC/ATNI 2019/16, https://www.eionet.europa.eu/etcs/etc-atni/products/etc-atni-reports/etc-atni-report-16-2019-air-quality-trends-in-europe-2000-2017-assessment-for-surface-so2-no2-ozone-pm10-and-pm2-5-1, 2021.

Considine, E. M., Reid, C. E., Ogletree, M. R., and Dye, T.: Improving accuracy of air pollution exposure measurements: Statistical correction of a municipal low-cost airborne particulate matter sensor network, Environmental Pollution, 268, 115 833, https://doi.org/https://doi.org/10.1016/j.envpol.2020.115833, 2021.

Crilley, L. R., Shaw, M., Pound, R., Kramer, L. J., Price, R., Young, S., Lewis, A. C., and Pope, F. D.: Evaluation of a low-cost optical particle counter (Alphasense OPC-N2) for ambient air monitoring, Atmospheric Measurement Techniques, 11, 709–720, https://doi.org/10.5194/amt-11-709-2018, 2018.

Degefie, D., El-Madany, T.-S., Hejkal, J., Held, M., Dupont, J.-C., Haeffelin, M., and Klemm, O.: Microphysics and energy and water fluxes of various fog types at SIRTA, France, Atmospheric Research, 151, 162–175, https://doi.org/https://doi.org/10.1016/j.atmosres.2014.03.016, sixth International Conference on Fog, Fog Collection and Dew, 2015.

Elias, T., Haeffelin, M., Drobinski, P., Gomes, L., Rangognio, J., Bergot, T., Chazette, P., Raut, J., and Colomb, M.: Extinction of Light during the Fog Life Cycle: a Result from the ParisFog Experiment, AIP Conference Proceedings, 1100, 165–168, https://doi.org/10.1063/1.3116939, 2009a.

Elias, T., Haeffelin, M., Drobinski, P., Gomes, L., Rangognio, J., Bergot, T., Chazette, P., Raut, J.-C., and Colomb, M.: Particulate contribution to extinction of visible radiation: Pollution, haze, and fog, Atmospheric Research, 92, 443–454, https://doi.org/https://doi.org/10.1016/j.atmosres.2009.01.006, 2009b.

Feinberg, S. N., Williams, R., Hagler, G., Low, J., Smith, L., Brown, R., Garver, D., Davis, M., Morton, M., Schaefer, J., and Campbell, J.: Examining spatiotemporal variability of urban particulate matter and application of high-time resolution data from a network of low-cost air pollution sensors, Atmospheric Environment, 213, 579–584, https://doi.org/https://doi.org/10.1016/j.atmosenv.2019.06.026, 2019.

380 Girdwood, J., Smith, H., Stanley, W., Ulanowski, Z., Stopford, C., Chemel, C., Doulgeris, K.-M., Brus, D., Campbell, D., and Mackenzie, R.: Design and field campaign validation of a multi-rotor unmanned aerial vehicle and optical particle counter, Atmospheric Measurement Techniques, 13, 6613–6630, https://doi.org/10.5194/amt-13-6613-2020, 2020.

Gultepe, I., Tardif, R., Michaelides, S., Cermak, J., Bott, A., Muller, M., Pagowski, M., Hansen, B., Ellrod, G., Jacobs, W., Toth, G., and Cober, S.: Fog research: A review of past achievements and future perspectives., Pure and Applied Geophysics, 164, 1121–1159, 2007.

385 Gultepe, I., Pearson, G., Milbrandt, J. A., Hansen, B., Platnick, S., Taylor, P., Gordon, M., Oakley, J. P., and Cober, S. G.: The Fog Remote Sensing and Modeling Field Project, Bulletin of the American Meteorological Society, 90, 341 – 360, https://doi.org/10.1175/2008BAMS2354.1, 2009.

Gultepe, I., Zhou, B., Milbrandt, J., Bott, A., Li, Y., Heymsfield, A., Ferrier, B., Ware, R., Pavolonis, M., Kuhn, T., Gurka, J., Liu, P., and Cermak, J.: A review on ice fog measurements and modeling, Atmospheric Research, 151, 2–19, 390 https://doi.org/https://doi.org/10.1016/j.atmosres.2014.04.014, sixth International Conference on Fog, Fog Collection and Dew, 2015.

Gultepe, I., Heymsfield, A., Fernando, H., Pardyjak, E., Dorman, C., Wang, Q., Creegan, E., Hoch, S., Flagg, D., Yamaguchi, R., Krishna-murthy, R., Gabersek, S., Perrie, W., Perelet, A., Singh, D., Chang, R., Nagare, B., Wagh, S., and Wang, S.: A Review of Coastal Fog Microphysics During C-FOG, Boundary-Layer Meteorology, 181, 1–39, https://doi.org/10.1007/s10546-021-00659-5, 2021.

Habeck, J. B., Hogan, C. J., Flaten, J. A., and Candler, G. V.: Development of a calibration system for measuring aerosol particles in the 395 stratosphere, in: AIAA SCITECH 2022 Forum, p. 1582, 2022.

Haeffelin, M., Bergot, T., Elias, T., Tardif, R., Carrer, D., Chazette, P., Colomb, M., Drobinski, P., Dupont, E., Dupont, J.-C., Gomes, L., Musson-Genon, L., Pietras, C., Plana-Fattori, A., Protat, A., Rangognio, J., Raut, J.-C., Rémy, S., Richard, D., Sciare, J., and Zhang, X.: Parisfog: Shedding new Light on Fog Physical Processes, Bulletin of the American Meteorological Society, 91, 767 – 783, https://doi.org/10.1175/2009BAMS2671.1, 2010.

400 Hagan, D. H. and Kroll, J. H.: Assessing the accuracy of low-cost optical particle sensors using a physics-based approach, Atmospheric Measurement Techniques, 13, 6343–6355, https://doi.org/10.5194/amt-13-6343-2020, 2020.

Hale, G. M. and Querry, M. R.: Optical Constants of Water in the 200-nm to 200-μm Wavelength Region, Appl. Opt., 12, 555–563, https://doi.org/10.1364/AO.12.000555, 1973.

Hamazu, K., Hashiguchi, H., Wakayama, T., Matsuda, T., Doviak, R. J., and Fukao, S.: A 35-GHz Scanning Doppler 405 Radar for Fog Observations, Journal of Atmospheric and Oceanic Technology, 20, 972 – 986, https://doi.org/10.1175/1520-0426(2003)20<972:AGSDRF>2.0.CO;2, 2003.

Hu, H., Sun, J., and Zhang, Q.: Assessing the Impact of Surface and Wind Profiler Data on Fog Forecasting Using WRF 3DVAR: An OSSE Study on a Dense Fog Event over North China, Journal of Applied Meteorology and Climatology, 56, 1059 – 1081, https://doi.org/10.1175/JAMC-D-16-0246.1, 2017.

410 Jayaratne, R., Liu, X., Thai, P., Dunbabin, M., and Morawska, L.: The influence of humidity on the performance of a low-cost air particle mass sensor and the effect of atmospheric fog, Atmospheric Measurement Techniques, 11, 4883–4890, https://doi.org/10.5194/amt-11-4883-2018, 2018.

Kashdan, J. T., Shrimpton, J. S., and Whybrew, A.: Two-Phase Flow Characterization by Automated Digital Image Analysis. Part 1: Fundamental Principles and Calibration of the Technique, Particle & Particle Systems Characterization, 20, 387–397, https://doi.org/https://doi.org/10.1002/ppsc.200300897, 2003.

Kashdan, J. T., Shrimpton, J. S., and Whybrew, A.: Two-Phase Flow Characterization by Automated Digital Image Analysis. Part 2: Application of PDIA for Sizing Sprays, Particle & Particle Systems Characterization, 21, 15–23, https://doi.org/https://doi.org/10.1002/ppsc.200400898, 2004.

Klemm, O. and Lin, N.-H.: What Causes Observed Fog Trends: Air Quality or Climate Change?, Aerosol and Air Quality Research, 16, 1131–1142, https://doi.org/10.4209/aaqr.2015.05.0353, 2016.

Kulkarni, R., Jenamani, R. K., Pithani, P., Konwar, M., Nigam, N., and Ghude, S. D.: Loss to Aviation Economy Due to Winter Fog in New Delhi during the Winter of 2011–2016, Atmosphere, 10, https://doi.org/10.3390/atmos10040198, 2019.

Liu, D., Yang, J., Niu, S., and Li, Z.: On the Evolution and Structure of a Radiation Fog Event in Nanjing, Advances in Atmospheric Sciences, 28, 223–237, https://doi.org/10.1007/s00376-010-0017-0, 2011.

Liu, H.-Y., Schneider, P., Haugen, R., and Vogt, M.: Performance Assessment of a Low-Cost PM2.5 Sensor for a near Four-Month Period in Oslo, Norway, Atmosphere, 10, https://doi.org/10.3390/atmos10020041, 2019.

Maalick, Z., Kühn, T., Korhonen, H., Kokkola, H., Laaksonen, A., and Romakkaniemi, S.: Effect of aerosol concentration and absorbing aerosol on the radiation fog life cycle, Atmospheric Environment, 133, 26–33, https://doi.org/https://doi.org/10.1016/j.atmosenv.2016.03.018, 2016.

Martinet, P., Cimini, D., Burnet, F., Ménétrier, B., Michel, Y., and Unger, V.: Improvement of numerical weather prediction model analysis during fog conditions through the assimilation of ground-based microwave radiometer observations: a 1D-Var study, Atmospheric Measurement Techniques, 13, 6593–6611, https://doi.org/10.5194/amt-13-6593-2020, 2020.

Martinet, P., Burnet, F., Bell, A., Kremer, A., Letillois, M., Löhnert, U., Antoine, S., Caumont, O., Cimini, D., Delanöe, J., Hervo, M., Huet, T., Georgis, J.-F., Orlandi, E., Price, J., Raynaud, L., Rottner, L., Seity, Y., , and Unger, V.: Benefit of microwave radiometer and cloud radar observations for data assimilation and fog process studies during the SOFOG3D experiment, in: EMS Annual Meeting 2021, online, 6–10 Sep 2021, EMS2021-232, https://doi.org/https://doi.org/10.5194/ems2021-232, 2021.

Mazoyer, M., Burnet, F., Denjean, C., Roberts, G. C., Haeffelin, M., Dupont, J.-C., and Elias, T.: Experimental study of the aerosol impact on fog microphysics, Atmospheric Chemistry and Physics, 19, 4323–4344, https://doi.org/10.5194/acp-19-4323-2019, 2019.

Mazoyer, M., Burnet, F., and Denjean, C.: Experimental study on the evolution of droplets size distribution during the fog life cycle, Atmospheric Chemistry and Physics Discussions, 2022, 1–28, https://doi.org/10.5194/acp-2021-1027, 2022.

Mohammadi, M., Nowak, J. L., Bertens, G., Moláček, J., Kumala, W., and Malinowski, S. P.: Cloud microphysical measurements at a mountain observatory: comparison between shadowgraph imaging and phase Doppler interferometry, Atmospheric Measurement Techniques, 15, 965–985, https://doi.org/10.5194/amt-15-965-2022, 2022.

Nowak, J. L., Mohammadi, M., and Malinowski, S. P.: Applicability of the VisiSize D30 shadowgraph system for cloud microphysical measurements, Atmospheric Measurement Techniques, 14, 2615–2633, https://doi.org/10.5194/amt-14-2615-2021, 2021.

Posyniak, M., Markowicz, K., Czyzewska, D., Chilinski, M., Makuch, P., Zawadzka-Manko, O., Kucieba, S., Kulesza, K., Kachniarz, K., Mijal, K., and Borek, K.: Experimental study of smog microphysical and optical vertical structure in the Silesian Beskids, Poland, Atmospheric Pollution Research, 12, 101 171, https://doi.org/https://doi.org/10.1016/j.apr.2021.101171, 2021.

Price, J. D., Lane, S., Boutle, I. A., Smith, D. K. E., Bergot, T., Lac, C., Duconge, L., McGregor, J., Kerr-Munslow, A., Pickering, M., and Clark, R.: LANFEX: A Field and Modeling Study to Improve Our Understanding and Forecasting of Radiation Fog, Bulletin of the American Meteorological Society, 99, 2061 – 2077, https://doi.org/10.1175/BAMS-D-16-0299.1, 2018.

Pruppacher, H. and Klett, J.: Microstructure of Atmospheric Clouds and Precipitation, pp. 10–73, Springer Netherlands, Dordrecht, https://doi.org/10.1007/978-0-306-48100-0_2, 2010.

Tsai, I.-C., Hsieh, P.-R., Cheung, H. C., and Chung-Kuang Chou, C.: Aerosol impacts on fog microphysics over the western side of Taiwan Strait in April from 2015 to 2017, Atmospheric Environment, 262, 118 523, https://doi.org/https://doi.org/10.1016/j.atmosenv.2021.118523, 2021.

Vautard, R., Yiou, P., and Van Oldenborgh, G. J.: Decline of fog, mist and haze in Europe over the past 30years, Nature Geoscience - NAT GEOSCI, 2, 115–119, https://doi.org/10.1038/ngeo414, 2009.

Vishwakarma, P., Delanoë, J., Le Gac, C., Bertrand, F., Dupont, J.-C., Haeffelin, M., Martinet, P., Burnet, F., Lac, C., Bell, A., Vignelles, D., Toledo, F., Jorquera, S., and Vinson, J.-P.: Fog Analysis during SOFOG3D Experiment, in: vEGU General Assembly 2021, online, 19–30 Apr 2021, EGU21-9941, https://doi.org/https://doi.org/10.5194/egusphere-egu21-9941, 2021.

Wang, Q., Yamaguchi, R. T., Kalogiros, J. A., Daniels, Z., Alappattu, D. P., Jonsson, H., Alvarenga, O., Olson, A., Wauer, B. J., Ortiz-Suslow, D. G., and Fernando, H. J.: Microphysics and Optical Attenuation in Fog: Observations from Two Coastal Sites, Boundary-Layer Meteorology, 181, 267–292, https://doi.org/10.1007/s10546-021-00675-5, 2021.

Wang, Y., Li, J., Jing, H., Zhang, Q., Jiang, J., and Biswas, P.: Laboratory Evaluation and Calibration of Three Low-Cost Particle Sensors for Particulate Matter Measurement, Aerosol Science and Technology, 49, 1063–1077, https://doi.org/10.1080/02786826.2015.1100710, 2015.

Weston, M., Francis, D., Nelli, N., Fonseca, R., Temimi, M., and Addad, Y.: The First Characterization of Fog Microphysics in the United Arab Emirates, an Arid Region on the Arabian Peninsula, Earth and Space Science, 9, e2021EA002 032, https://doi.org/https://doi.org/10.1029/2021EA002032, e2021EA002032 2021EA002032, 2022.

Wærsted, E., Haeffelin, M., Dupont, J.-C., Delanoë, J., and Dubuisson, P.: Radiation in fog: Quantification of the impact on fog liquid water based on ground-based remote sensing, Atmospheric Chemistry and Physics, 17, 10 811–10 835, https://doi.org/10.5194/acp-17-10811-2017, 2017.